Check for updates

Interplay between transition-metal K-edge XMCD, slight structural distortions and magnetism in a series of trimetallic (Co$_x$Ni$_{(1−x)}$)$_4$[Fe(CN)$_6$]$_{3/8}$ Prussian blue analogues†

Adama N'Diaye,[a] Amélie Bordage, [ID][a] Lucie Nataf,[b] François Baudelet,[b] Eric Rivière [ID][a] and Anne Bleuzen [ID] *[a]

The magnetic properties of a series of trimetallic (Co,Ni)Fe Prussian blue analogues (PBAs) were investigated by SQUID magnetometry and X-ray magnetic circular dichroism (XMCD) at the three transition metal (TM) K-edges. In turn, the PBA trimetallic series was used as a tool in order to better understand the information contained in TM K-edge XMCD and particularly the chemical nature of the probed species (extended sub-lattice or localized entities). The results show that the magnetic behavior of the compounds is dictated by competing exchange interactions between the Co–Fe and Ni–Fe pairs, without spin frustration. They also show that XMCD at the TM K-edge is a local atomic probe of the element at the N side of the cyanide bridge and a local probe of the absorbing atom and its first magnetic neighbors on the C side of the bridge. At last, XMCD at the TM K-edge turns out to be highly sensitive to very small structural distortions.

Introduction

X-ray magnetic circular dichroism (XMCD) at the transition metal (TM) K-edge is less frequently used than XMCD at the TM L$_{2,3}$ edges as a local magnetic probe. Indeed, in contrast to XMCD at the L$_{2,3}$ edges of TMs, for which quantitative information can be extracted from the sum rules[1–3] and the spectra can be well-reproduced by crystal field multiplet calculations,[4] the interpretation of the XMCD signals at the TM K-edge remains unsatisfactory despite many efforts towards the quantitative interpretation and the reproduction of the signals.[5–15] Yet, XMCD at the TM K-edge is the preferred technique to probe magnetism under pressure for instance.[16–21] The literature on XMCD at the TM K-edge mostly deals with the study of metals,[22] metal alloys[23] and intermetallics,[24,25] while works dealing with the study of molecular compounds are scarcer.

Most studies of molecular compounds by XMCD at the TM K-edge deal with the investigation of Prussian blue analogues (PBAs). Noticeably, in the search for room-temperature molecular-based magnets, Verdaguer and his team used this

technique in the 90's as a probe of the exchange interactions in PBAs: they related the sign of the TM K-edge XMCD signal to the orientation of the magnetic moment carried by the absorbing atom with respect to the applied magnetic field.[26–33] Since then, only qualitative information has been extracted from these signals.

Therefore, we are engaged in the project aiming at disentangling the physical effects at the origin of the TM K-edge XMCD signals. We have been developing an original experimental approach aiming at making TM K-edge XMCD a real quantitative tool for molecular chemists.[34–38] Our strategy, presented in previous works,[35–38] uses the versatile chemistry of PBAs exhibiting the well-known face-centered cubic (fcc) structure, the unit cell of which is shown in Fig. 1 (for p = 4 and q = 8/3) and the chemical composition per unit cell is given by A$_p$[B(CN)$_6$]$_q$·nH$_2$O, where A and B are two TM ions. The large variety of TM ions that can thus be combined in isostructural compounds allow for the independent variation of the magnetic orbitals on both A and B sites. This enables the analysis of the effect of a change of each of them on both TM K-edge XMCD signals. Thus, the analysis of the TM K-edge XMCD signals of two series of PBAs of chemical formula A$_4^{II}$[Fe^{III}(CN)$_6$]$_{3/8}$·nH$_2$O (A^{2+} = Mn^{2+}, Co^{2+}, Ni^{2+}, Cu^{2+}) and A$_4^{II}$[Cr^{III}(CN)$_6$]$_{3/8}$·nH$_2$O (A^{2+} = Mn^{2+}, Fe^{2+}, Co^{2+}, Ni^{2+}) showed that TM K-edge XMCD was very sensitive to orbital symmetry and allowed us to relate the main 1s → 4p contribution of the XMCD signal to the electronic structure and the magnetic

[a] *Institut de Chimie Moléculaire et des Matériaux d'Orsay, Université Paris-Saclay, CNRS, 91405 Orsay, France. E-mail: anne.bleuzen@universite-paris-saclay.fr*

[b] *Synchrotron SOLEIL, L'Orme des Merisiers, St Aubin, BP 48, 91192 Gif sur Yvette, France*

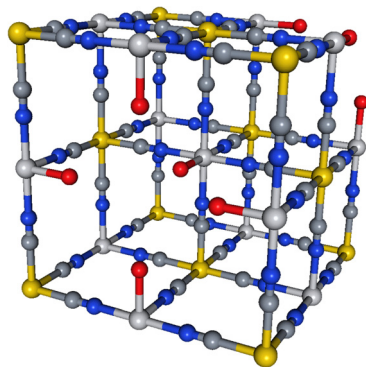† Electronic supplementary information (ESI) available. See DOI: https://doi.org/10.1039/d3cp04749k

15576 | *Phys. Chem. Chem. Phys.*, 2024, **26**, 15576–15586

This journal is © the Owner Societies 2024

Fig. 1 Scheme of the unit cell of a Prussian blue analogue with the chemical formula $A_4[B(CN)_6]_{2.7} \cdot x H_2O$. Yellow circles stand for the B^{3+} ion, light grey circles the A^{2+} ions, dark grey the carbon atoms, blue the nitrogen atoms, and red the oxygen atoms. The hydrogen atoms of the water molecules bonded to the A^{2+} ions as well as the zeolitic water molecules are omitted for clarity.

behavior of (i) the probed ion on the N side of the cyanide bridge and (ii) the probed ion and its magnetic neighbors on the C side. Furthermore, an expression for the intensity of this main 1s → 4p contribution was unprecedently derived for the sixteen XMCD signals (at both TM K-edges of the eight PBAs) of the two series.[36,38] This study also showed that XMCD at the TM K-edge can provide both original local structural and magnetic information, which, combined with macroscopic magnetic measurements, allowed for an unprecedented in-depth analysis of the magnetic behaviors of the two bimetallic series of PBAs.

In this work, we now focus on a series of trimetallic PBAs. Twenty-five years ago, trimetallic PBAs generated interest because of their intriguing magnetic behaviors and particularly magnetic pole inversions due to competitive exchange inter-actions between the TM ions[39–47] and also, later on, some photo-switching properties;[48–50] their magnetic properties were essentially investigated by SQUID magnetometry at the macro-scopic level. In our on-going commitment to promote TM K-edge XMCD as a regular local probe of TM magnetic moment in molecular compounds, these systems offer the opportunity to go ahead. On the one hand, such study of trimetallic PBAs is an opportunity to test the relevancy of TM K-edge XMCD for the study of the magnetic properties of more complex systems than bimetallic PBAs. On the other hand, with the aim to better understand the information contained in the XMCD signals, one can analyze the effect on the XMCD signal at the three TM K-edges of the replacement of one ion by another in varying amounts in the same sublattice of one PBA; this should provide information on the nature of the species probed (extended on a sublattice level or localized at the atomic scale). Among trimetallic PBAs, the series of chemical formula $(Co_xNi_{(1-x)})_4[Fe(CN)_6]_{8/3} \cdot nH_2O$ (where x is the mole fraction of Co ions on the A site of the alkali cation free NiFe PBA), called the $Co_xNi_{(1-x)}Fe$ series in the following, has been chosen. The preparation of the samples and their characterization are given in the experimental part and the ESI† (S1–S3). For this study, K-edge XMCD has a great advantage compared with L-edge

XMCD, which is yet a direct local probe of the 3d levels: the former is bulk sensitive like SQUID magnetometry and there-fore little sensitive to surface effects. Surface effects, which are yet poorly understood in PBAs, can be detected by surface sensitive techniques such as L-edge XMCD. Thus, the parent Rb-containing photo-switchable RbCoFe PBA of chemical formula $Rb_2Co_4[Fe(CN)_6]_{3.3} \cdot 11H_2O$ was already studied by L-edge XMCD.[51] This study revealed weak ferromagnetic interaction at the surface of the ferrimagnetic photoexcited state of RbCoFe.[51] The addition to the XMCD signal of yet poorly understood surface effects could blur the information being sought here, making K-edge XMCD the most appropriate choice for this study. At last, it has also to be mentioned that neither experi-mental nor theoretical studies on the relative orientation of the magnetic moments on the A and B sites of the $Co_xNi_{(1-x)}Fe$ series are available in the literature.

Results

Magnetic measurements

The magnetization curves *versus* the magnetic field at 4 K, temperature at which the XMCD measurements were per-formed, are shown in Fig. 2 for the samples of the $Co_xNi_{(1-x)}Fe$ series.

The field cooled (FC) and zero field cooled (ZFC) magnetiza-tion curves, as well as the temperature dependence of the inverse of magnetic molar susceptibilities, are given in S2 and S3 (ESI†). The magnetic ordering temperature $T_{C/N}$ was deter-mined as the temperature of a minimum in the derivative of the FC magnetization curve ($dM_{FC}(T)/dT$; S2, ESI†). The Weiss (θ) magnetic constant was extracted from the plots of the inverse of the molar susceptibility *versus* temperature by fitting a Curie–Weiss law to the curves (S3, ESI†). All these magnetic data as well as the coercive field (H_C) at 4 K and the magnetization value at 4 K and 4 T are gathered in Table 1.
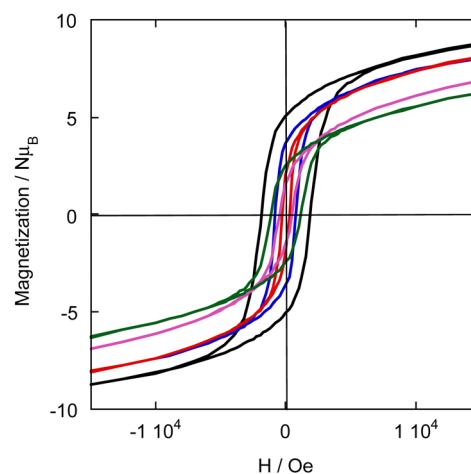

Fig. 2 Magnetic field dependence of the magnetization at 4 K of CoFe (green), $Co_{0.7}Ni_{0.3}Fe$ (pink), $Co_{0.56}Ni_{0.44}Fe$ (red), $Co_{0.35}Ni_{0.65}Fe$ (blue), and NiFe (black).

This journal is © the Owner Societies 2024

Phys. Chem. Chem. Phys., 2024, **26**, 15576–15586 | **15577**

Table 1 Macroscopic magnetic parameters of CoFe, $Co_{0.7}Ni_{0.3}Fe$, $Co_{0.56}Ni_{0.44}Fe$, $Co_{0.35}Ni_{0.65}Fe$, and NiFe

	$T_{C/N}$ (K)	θ (K)	H_c ($\times 10^{-4}$ T)	M (4 T) ($N\mu_B$)	$M_{sat\,calc}$ powder mixture ($N\mu_B$)	$M_{sat\,calc}$ ($N\mu_B$)
CoFe	14	−9	1240	8.3	9.3	9.3
$Co_{0.7}Ni_{0.3}Fe$	12	−0.25	500	8.9	9.7	3.3
$Co_{0.56}Ni_{0.44}Fe$	12	8.3	250	9.7	9.9	0.5
$Co_{0.35}Ni_{0.65}Fe$	16	14	750	9.4	10.2	3.7
NiFe	22	32	2000	10.1	10.7	10.7

The FC/ZFC magnetization curves (S2, ESI†) show the classical profile of PBA magnets and they show that at 4 K, temperature at which the XMCD signals were recorded, all compounds are in a magnetically ordered state. The single X-ray diffraction peak for each reflection (S1), the unique minimum exhibited by the $dM_{FC}(T)/dT$ curve (S2, ESI†) and the profile of the magnetic field dependence of the magnetization (Fig. 2) show that all compounds are made of a homogeneous PBA phase mixing the Ni^{2+} and Co^{2+} ions at the atomic scale. The presence of several phases richer in one or the other ion can be excluded.

As a first approximation, for TM ions of the first row, magnetic moments are considered originating from the spin angular momentum only. In the magnetically ordered states of PBAs, the orientation of the magnetic moments with regard to an applied external magnetic field can thus generally be predicted from the total spin quantum number of the ions and from the sign of J. In bimetallic PBAs, the magnetic moment of the ion with the largest total spin quantum number aligns in the direction of the magnetic field and the second one is parallel ($J > 0$) or antiparallel ($J < 0$) to the former depending on the sign of J. In such compounds where exchange interactions prevail, the sign of θ directly gives the sign of J. Thus, CoFe is a ferrimagnet: the magnetic moment carried by the Co^{2+} ion aligns in the direction of the applied magnetic field and the one of the Fe^{3+} ion in the opposite direction (Fig. 3a).[36] In contrast, NiFe is a ferromagnet: the magnetic moments carried by both the Ni^{2+} and the Fe^{3+} ions align in the direction of the applied magnetic field (Fig. 3b).[36]

In trimetallic PBAs containing two different metal ion pairs with different nature of exchange interactions (antiferro- and ferromagnetic) between them, the situation is more complex. As mentioned in the introductory part, several examples of magnetic studies of trimetallic PBAs exist in the literature and especially the PBA series of chemical formula $(Mn_xNi_{(1-x)})_4$-$[Cr(CN)_6]_{8/3}\cdot nH_2O$,[39–42] called the $Mn_xNi_{(1-x)}Cr$ series in the following. This trimetallic PBA series is comparable to our series as the extreme compounds MnCr and NiCr are also respectively ferrimagnet and ferromagnet. For this $Mn_xNi_{(1-x)}Cr$ series, the saturation magnetization was well predicted along the series by considering the same exchange interaction as in the extreme bimetallic compounds between the same pairs of ions. In the same way, we tried to predict the saturation magnetization value for one unit cell for the compounds of the $Co_xNi_{(1-x)}Fe$ series by considering the same exchange interaction as in the bimetallic extreme PBAs between the same ion pairs (Fig. 3c) using eqn (1) in $N\mu_B$ units, where N is the Avogadro constant, μ_B the Bohr
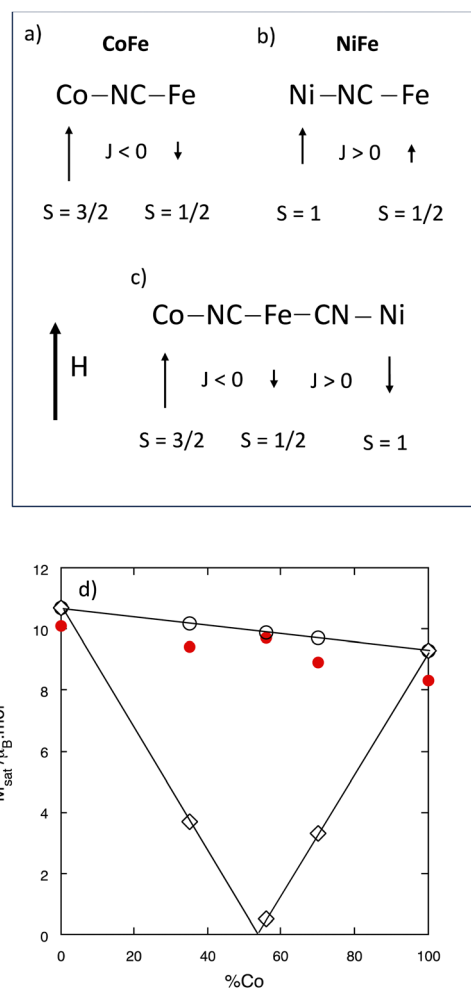

Fig. 3 Scheme of the orientation of the magnetic moment borne by the TM ions in an applied magnetic field H for (a) CoFe, (b) NiFe and (c) the $Co_xNi_{(1-x)}Fe$ series by considering the same magnetic behavior as in the $Mn_xNi_{(1-x)}Cr$ series.[39–42] (d) Experimental magnetization value at 4 K and 4 T (red circle) for the $Co_xNi_{(1-x)}Fe$ series and M_{sat} values as a function of x calculated from eqn (1) (white diamond) and for the corresponding mixture of the CoFe and NiFe PBA powders (white circle).

magneton and g the electron g-factor ($g = 2$) and which is equivalent to the equation used in ref. 39–42:

$$M_{sat\,calc} = g\left|4(xS_{Co} - (1-x)S_{Ni}) - 8/3S_{Fe}\right| \qquad (1)$$

The calculated values ($M_{sat\,calc}$) are given in Table 1 and plotted as a function of x in Fig. 3d, where they are compared to the experimental magnetization values at 4 T and the values calculated for the corresponding mixture of the CoFe and NiFe

15578 | *Phys. Chem. Chem. Phys.*, 2024, **26**, 15576–15586

This journal is © the Owner Societies 2024

PBA powders. Even if the saturation is not reached at 4 T, Fig. 3d clearly shows that eqn (1) fails to predict the experimental saturation magnetization in our $Co_xNi_{(1-x)}Fe$ series. The magnetic behavior of our $Co_xNi_{(1-x)}Fe$ series is therefore different from that of the $Mn_xNi_{(1-x)}Cr$ one described in ref. 39–42. To get a better insight into this original magnetic behavior, the compounds of the $Co_xNi_{(1-x)}Fe$ series were investigated by XMCD at the Co, Ni and Fe K-edges to probe the local magnetic moment on each TM ion.

XMCD at the Co and Ni K-edges

The XMCD signals at the Co and Ni K-edges for the $Co_xNi_{(1-x)}Fe$ series are shown in Fig. 4a and b respectively.

The Co and Ni ions occupy the same site of the fcc PBA structure, called the A site above and in ref. 36. For this A site, the contributions to the signal over the edge and pre-edge regions were already assigned and discussed in ref. 36 and 38. For all compounds, over the pre-edge and edge regions, the XMCD signal exhibits one main contribution (γ) and two other contributions of significantly smaller intensity (α and β), all situated at the same energies along the series. The α contribution can be assigned to the electric-dipole forbidden 1s → 3d transitions and explained by the low symmetry of the site and associated 3d–4p orbital mixing. The β contribution can be assigned to the 1s → $t_{1u}CN\pi^*$ transitions. The two latter contributions will not be further discussed here. The main contribution to the XMCD signal (γ) at the Co K-edge (Fig. 4a) and at the Ni K-edge (Fig. 4b) can be assigned to the electric-dipole allowed 1s → 4p transitions. For one given K-edge, its intensity is very close from one compound to the other and very close to that of the corresponding bimetallic PBA, except the one of $Co_{0.35}Ni_{0.65}Fe$, which is significantly higher at both edges (blue curves). It is now well established that the sign of the main contribution to the XMCD signal in PBAs is directly related to the nature of the exchange interaction between the TM, *i.e.* to the direction of the magnetic moment of the probed atom with regard to the applied magnetic field.[18,30,31,36,38] The same sign and the same intensity of the main contribution for CoFe, $Co_{0.7}Ni_{0.3}Fe$ and $Co_{0.56}Ni_{0.44}Fe$ at the Co K-edge on the one hand and for NiFe, $Co_{0.7}Ni_{0.3}Fe$ and $Co_{0.56}Ni_{0.44}Fe$ at the Ni K-edge on the other hand shows that the magnetic moment borne by the Co(Ni) ions as well as its direction is the same as that of the Co(Ni) ion in the corresponding bimetallic PBA, in line with the magnetic data. One can therefore conclude that, as in the corresponding bimetallic PBA, the magnetic moment of the Co(Ni) ions is aligned in the direction of the magnetic field.

The intensity of the main contribution to the XMCD signal of $Co_{0.35}Ni_{0.65}Fe$ is significantly higher (25–30%) than that of all other compounds at both the Co and Ni K-edges. This different behavior of $Co_{0.35}Ni_{0.65}Fe$ arises from different local features of the Co and Ni ions in this compound. The magnetic measurements do not reveal neither a different electronic structure of the Co^{2+} and Ni^{2+} ions in $Co_{0.35}Ni_{0.65}Fe$ nor a discontinuity in the macroscopic magnetic properties of this compound along the series. Nevertheless, structural strains and slight

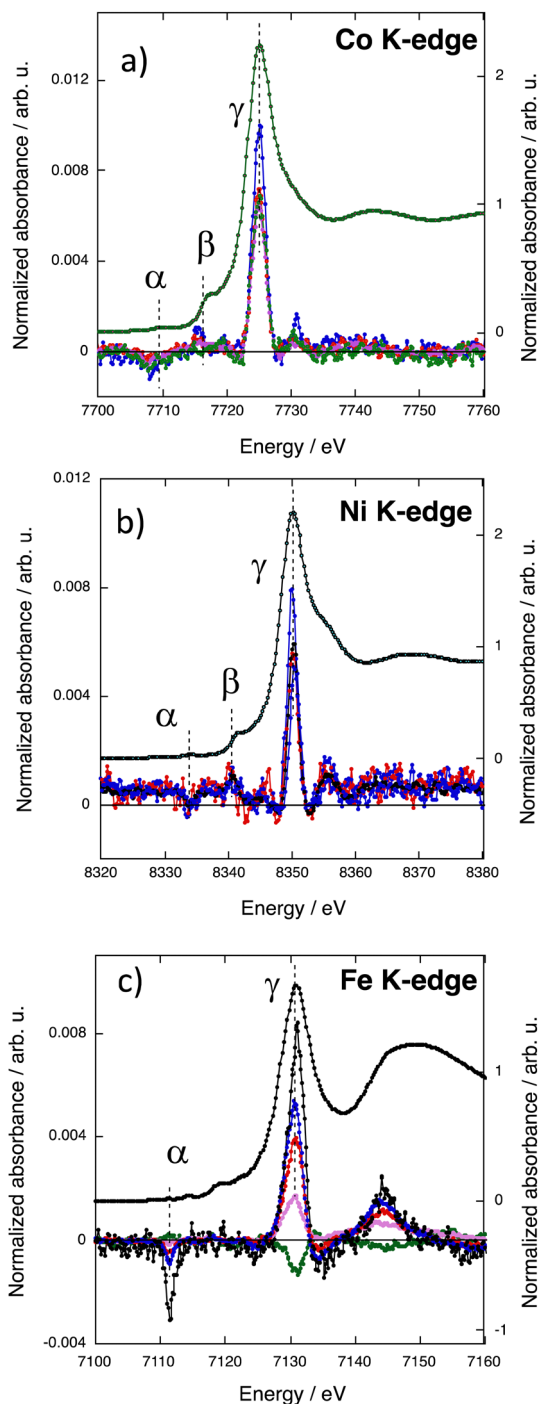**Fig. 4** XMCD signals of CoFe (green), $Co_{0.7}Ni_{0.3}Fe$ (pink), $Co_{0.56}Ni_{0.44}Fe$ (red), $Co_{0.35}Ni_{0.65}Fe$ (blue), and NiFe (black) (a) at the Co K-edge, (b) at the Ni K-edge and (c) at the Fe K-edge.

distortions of the ion coordination sphere could arise from the different sizes of the Co^{2+} and Ni^{2+} ions associated in the same A site of the PBA structure. The XRD patterns (S1) show that all compounds crystallize with the same fcc PBA structure and only the lattice constant varies. The variation of the lattice constant value with the percentage of Co^{2+} ions in the A site (Co%) is shown in Fig. S4 (ESI†). The lattice constant varies linearly with

This journal is © the Owner Societies 2024

Phys. Chem. Chem. Phys., 2024, **26**, 15576–15586 | **15579**

Co% for CoFe, $Co_{0.70}Ni_{0.30}Fe$ and $Co_{0.56}Ni_{0.44}Fe$, indicating that up to the replacement of 44% of Co^{2+} ions by the smaller Ni^{2+} ones, the PBA structure accommodates both ions by a decrease of the lattice constant. Nevertheless, one can also see that the lattice constant of NiFe deviates from this linear variation as well as that of $Co_{0.35}Ni_{0.65}Fe$. When the Co% reaches a certain threshold between 56 and 35%, the replacement of Co^{2+} ions by the Ni^{2+} ones can no more be compensated by a single lattice constant decrease. The size of both cations being different, one too small (Ni^{2+}) and the other one too large (Co^{2+}) for the ideal face centered cubic lattice, the structural distortion would be local and different for both ions. Network strains likely develop, slightly distorting the coordination spheres of the Co^{2+} and Ni^{2+} ions and enhancing the deviation from the pure O_h symmetry of the local structure of the ions either with a slight displacement of the ion from the crystallographic site and/or a slight tilt of the coordination polymer. Such a local distortion of the A site, by reinforcing the intra-site 3d–4p orbital mixing, could explain the higher intensity of the main contribution to the XMCD signal of $Co_{0.35}Ni_{0.65}Fe$ at the Co and Ni K-edges.

XMCD at the Fe K-edge

The XMCD signals of the $Co_xNi_{(1-x)}Fe$ series at the Fe K-edge are shown in Fig. 4c. All the spectra exhibit the same contributions. Over the pre-edge and edge regions, the α and γ contributions can be assigned to the 1s → 3d and the 1s → 4p transitions respectively.[38] It is striking that the intensity of the γ contribution at the Fe K-edge varies strongly with the Co%. We already showed in ref. 38 that the γ contribution at the TM K-edge at the B site is sensitive to the nature of the ion in the A site, on the contrary to the A site, which is not sensitive to the ions in the B site; this difference between both sites is explained by the different symmetries of the sites.[38] In ref. 38, we showed that the intensity of the main contribution to the XMCD signal at the Fe K-edge is well reproduced by eqn (2).

$$I^{Fe} = (1 \pm S_A) \times (1/3) \times P_{exp} \qquad (2)$$

where S_A is the total spin quantum number of the ion in the A site, the sign in front of S_A depends on the nature of the exchange interaction between the Fe ion and the TM ion in the A site (–(+) for an antiferromagnetic (ferromagnetic) exchange interaction), and P_{exp} is a constant, which depends on the experimental conditions (temperature, magnetic field, and the circular polarization rate of light). Under our experimental conditions, P_{exp} is equal to 0.012.[36,38] Eqn (2), in which $\pm S_A$ is replaced by $((1 - x)S_{Ni} - xS_{Co})$, is given by eqn (3).

$$I^{Fe} = (1 + (1 - x)S_{Ni} - xS_{Co}) \times (1/3) \times P_{exp} \qquad (3)$$

Eqn (3) has been used to predict the experimental intensity of the γ peak for our $Co_xNi_{(1-x)}Fe$ series. The plot of the experimental (I_{exp}) versus the calculated (I_{calc}) intensity using eqn (3) is shown in Fig. 5, where the plot of I_{exp} versus I_{calc} for the sixteen XMCD signals of the AFe PBAs (A^{2+} = Cu^{2+}, Ni^{2+}, Co^{2+}, Mn^{2+}) and the ACr PBAs (A^{2+} = Ni^{2+}, Co^{2+}, Fe^{2+}, Mn^{2+}) previously investigated and using the expressions for I_{calc} proposed in ref. 36 and 38 is also shown. Fig. 5 shows that the experimental
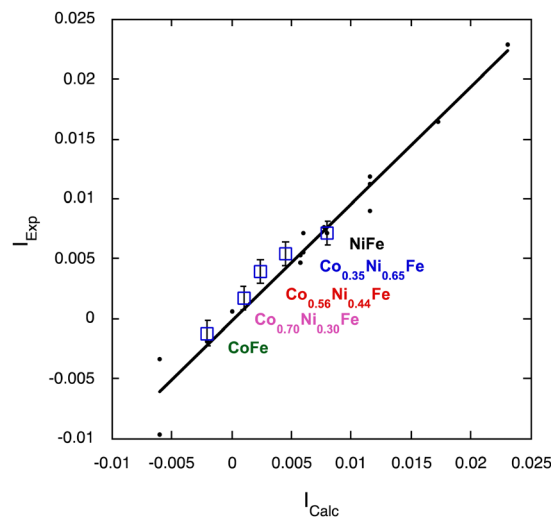

Fig. 5 Experimental (I_{exp}) versus calculated (I_{calc}) intensity using eqn (3) (blue open squares; error bar ±0.001) compared to I_{exp} versus I_{calc} for the sixteen XMCD signals of the AFe PBAs (A = Cu^{2+}, Ni^{2+}, Co^{2+}, Mn^{2+}) and the ACr PBAs (A = Ni^{2+}, Co^{2+}, Fe^{2+}, Mn^{2+}) previously investigated in ref. 36 and 38 (black dots).

intensity of the γ peak at the Fe K-edge is well reproduced by eqn (3) for all compounds of the $Co_xNi_{(1-x)}Fe$ series. This result shows that the behaviour of the Fe^{3+} ion magnetic moment in the trimetallic compounds is the same as the latter in the extreme bimetallic compounds (CoFe and NiFe) weighted by the amount of Co^{2+} and Ni^{2+} ions; it is antiferromagnetically coupled with the Co^{2+} ions and ferromagnetically coupled with the Ni^{2+} ones, resulting in the distribution of its magnetic moment over the two orientations weighted by the percentage of both Co^{2+} and Ni^{2+} ions in the compound.

Discussion

Input of this work on the understanding of the magnetic properties of PBAs

The behavior of the magnetic moments carried by all three TM ions (Co^{2+}, Ni^{2+} and Fe^{3+}) can be proposed from the XMCD investigation at the three TM K-edges.

Very close main contributions to the XMCD signal at the Co and Ni K-edges for $Co_{0.70}Ni_{0.30}Fe$, $Co_{0.56}Ni_{0.44}Fe$, CoFe and NiFe indicate that the magnetic moments carried by both ions exhibit the same behavior as in the extreme bimetallic compounds CoFe and NiFe. This means that the magnetic moments of the Co^{2+} and Ni^{2+} ions are aligned in the direction of the applied magnetic field. This is in agreement with the experimental values of the magnetization at 4 T, significantly higher than those calculated using eqn (1) considering antiparallel magnetic moments for the Co^{2+} and Ni^{2+} ions, as was the case for the Mn^{2+} and Ni^{2+} ions along the $Mn_xNi_{(1-x)}Cr$ series in ref. 39–42. The magnetic moments really borne by the Co^{2+} and Ni^{2+} ions are schematized as plain blue and plain green arrows in Fig. 6.
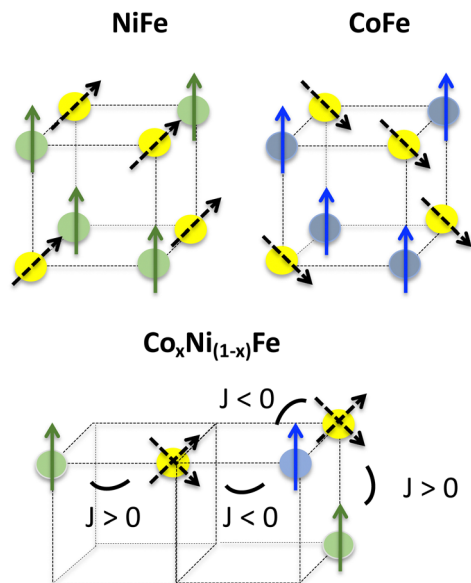
Fig. 6 Scheme of the proposed orientations of the magnetic moments for an octant of the fcc PBA structure. The Ni^{2+}, Co^{2+} and Fe^{3+} ions are represented by green, blue and yellow spheres, respectively, and their magnetic moments by plain green, plain blue and dotted black arrows. The orientations of the magnetic moment with regard to the crystallographic axes are those proposed in ref. 38. The proposed alignment of the Fe magnetic moments along the $\langle 111 \rangle$ directions is in line with a slight trigonal distortion of the $Fe(CN)_6$ entities[52] and a strong spin–orbit coupling. It has to be noted that the proposed spin-canted magnetic structure of the Fe ions remains a hypothesis or one of the possible models.

In the case of the Fe K-edge, the variation of the intensity of the main contribution to the XMCD signal is well reproduced by eqn (3). As mentioned above, this suggests that the behaviour of the Fe^{3+} ion magnetic moment in the trimetallic compounds is the same as that of the latter in the extreme bimetallic compounds, antiferromagnetically coupled with the Co^{2+} ions and ferromagnetically coupled with the Ni^{2+} ones but weighted by the amount of Co^{2+} and Ni^{2+} ions in the compounds. Such a magnetic situation could lead to spin frustration in the PBAs, especially since NiFe and CoFe present close strength of exchange interactions between the two ions in both ion pairs.‡[53] A frustration parameter given by $f = |\theta|/T_{C/N}$ has been introduced to evaluate the frustration degree and the condition $|\theta|/T_{C/N} > 10$ has been proposed as a criterion for the presence of frustration.[54] This empirical criterion was proposed assuming that magnetic interactions are on an energy

scale set by the exchange energy[54] and thus, without spin frustration, $|\theta|$ is expected to be close to the magnetic ordering temperature value. $|\theta|$ encompasses any deviation from the Curie law. In our case, deviation from the Curie law can reasonably be assigned to exchange interactions, but spin–orbit coupling can also play a non-negligible role. Assuming that neither NiFe nor CoFe exhibits spin frustration, the linear variation of the Curie–Weiss constant with the Co ion mole fraction percentage (x) along the series of compounds (Fig. S5, ESI†) shows that no significant effects other than those already operating in CoFe and NiFe are detectable along the series of compounds. Thus, along the $Co_xNi_{(1-x)}Fe$ series, the linear variation of θ with x (Fig. S5, ESI†), the low value of the f parameter ($f < 1.5$) for all compounds, the classical profile of the FC and ZFC magnetization curves, as well as the orientation of each pair of spins consistent with the sign of the corresponding J constant, allow us to rule out the presence of spin frustration in the compounds of the series, as it was the case for the $Mn_xNi_{(1-x)}Cr$ series previously studied.[39] From the variation of the intensity of the Fe K-edge XMCD signal (eqn (3)) along the $Co_xNi_{(1-x)}Fe$ series, we propose an orientation of the magnetic moments carried by the Fe^{3+} ions with regard to that of the applied magnetic field dictated by the weighted amount of both the Ni^{2+} and Co^{2+} ions in the A sub-lattice, without spin frustration. The direction and orientation of the magnetic moment borne by the Fe^{3+} ions under the influence of Co^{2+} or Ni^{2+} ions are schematized as black doted arrows in Fig. 6.

The main difference between the comparable $Mn_xNi_{(1-x)}Cr$ PBA series and our $Co_xNi_{(1-x)}Fe$ series is that, in the former, the orientation of the magnetic moments at low temperature is directly dictated by the exchange interaction between the two ions in each pair (Ni–Cr and Mn–Cr). On the contrary, in our series the magnetic moments of the Co^{2+} and Ni^{2+} ions at the A site both align in the direction of the magnetic field despite the different nature of exchange interactions with the Fe^{3+} ion that they surround, and then, the orientation of the magnetic moment carried by the Fe^{3+} ions is dictated by the exchange interactions between the two ions in both pairs (Ni–Fe and Co–Fe), the average orientation being dictated by the relative amount of both Co^{2+} and Ni^{2+} ions. These different magnetic behaviors of the $Mn_xNi_{(1-x)}Cr$ and $Co_xNi_{(1-x)}Fe$ PBA series arise from different magnetic behaviors of the TM ions listed below. First, due to the higher number of unpaired electrons in the t_{2g} orbitals for the Cr^{3+} ions (3 against 1 for the Fe^{3+} ions), the exchange interactions with the surrounding ions (Mn^{2+} and Ni^{2+}) are stronger in the $Mn_xNi_{(1-x)}Cr$ series than in the $Co_xNi_{(1-x)}Fe$ series. Second, due to the slightly different geometries of the $M(CN)_6$ entities, octahedral for $Cr(CN)_6$ and slightly trigonally distorted for $Fe(CN)_6$ with strong spin–orbit coupling (see ref. 38), the directions of the magnetic moments borne by the TM ion in these entities are different: aligned along the same $\langle 100 \rangle$ directions as those of the TM ions on the A site for the $Cr(CN)_6$ entities, while for the $Fe(CN)_6$ entities aligned along the $\langle 111 \rangle$ directions, different from those of the magnetic moments carried by the ions on the A site. Third, ref. 55 showing a comparable behavior of the $Cu_{0.73}Mn_{0.77}[Fe(CN)_6]\cdot zH_2O$

---

‡ The absolute value of the ratio between the magnetic coupling constant between both NiFe (J_{NiFe}) and CoFe (J_{CoFe}) ions pairs can be estimated within the mean-field approach by considering dominant exchange interaction between neighboring TM ions.[53] Indeed, the proportional relationship between $T_{C/N}$, the magnetic ordering temperature, z the number of magnetic neighbors and J the magnetic coupling constant for a given PBA is given by: $T_{C/N} \propto zJ$. The number of magnetic neighbors being the same in NiFe and CoFe, this approximation gives the value of 1.6 for $|J_{NiFe}/J_{CoFe}|$, indicative of exchange interactions with close strengths between both pairs of ions. Such close strength of exchange interactions of different nature in the same PBA network could give rise to spin frustration.

This journal is © the Owner Societies 2024

Phys. Chem. Chem. Phys., 2024, **26**, 15576–15586 | **15581**

compound to those of the Mn$_x$Ni$_{(1-x)}$Cr series, a stronger magnetic anisotropy of the Co^{2+} and Ni^{2+} ions in the Co$_x$Ni$_{(1-x)}$Fe series than that of the Mn^{2+} and Ni^{2+} ions in the Mn$_x$Ni$_{(1-x)}$Cr series can also be mentioned.[38] At last, one can also not exclude the role of the exchange interactions between TM second neighbors more important than those considered so far.

Input of this work on the understanding of XMCD at the transition metal K-edge for the study of molecular materials

1. Probed species. In a previous work,[36] we showed that the features of the main contribution to the XMCD signal at the TM K-edge of TM ions at the A site for the two AFe (A^{2+} = Cu^{2+}, Ni^{2+}, Co^{2+}, Mn^{2+}) and ACr (A^{2+} = Ni^{2+}, Co^{2+}, Fe^{2+}, Mn^{2+}) PBA series (i) do not depend on the nature of the TM ion at the B site and (ii) can be related to the electronic structure and magnetic behavior of the A^{2+} ion or of the A^{2+} ion sublattice: the shape of the signal to the filling of the 3d orbitals and the sign of the signal to the orientation of the magnetic moment with regard to that of the applied magnetic field; we also proposed an expression of its intensity as a function of the total spin quantum number S_A. The present study confirms the previous results and allows us to go a bit further concerning the species probed by XMCD at the A site of PBAs. As the intensity of the 1s → 4p XMCD contribution of CoFe at the Co K-edge is different from the one of NiFe at the Ni K-edge, the very close XMCD signals for the majority of the Co$_x$Ni$_{(1-x)}$Fe series at the Co(Ni) K-edge show that the 1s → 4p contribution to the XMCD signal at the K-edge of the ions on the A site is sensitive neither to the replacement of one ion by the other in the A ions sublattice nor to the average distance between the same ions of the A ion sublattice. Hence, XMCD at the K-edge of TM ions on the A site of the molecular PBA compounds is not a probe of the sublattice or of a part of the sublattice of the ions on the A site. In that case, the contribution to the signal of each absorbing atom, encompassing either the contribution of all other ions of the sublattice (overlap of all 4p orbitals of the A^{2+} ions) or the contribution of all other same atoms of the sublattice (overlap of all 4p orbitals of the probed Co^{2+} or Ni^{2+} ions), would vary with the chemical composition of the sublattice, which is not observed. On the contrary, XMCD at the K-edge of TM ions on the A site of the molecular PBA compounds is a local probe of each absorbing atom without any influence from other ions and the XMCD signal at the K-edge of the ions on the A site is the average of all their contributions.

The case of the B site is different because our previous work showed that the 1s → 4p XMCD signal at the K-edge of the ions on the B site of PBAs contains not only information on the ions or the sublattice of the ions on the B site but also on the ions on the A site.[38] In order to determine whether XMCD at the K-edge of ions at the B site of PBAs is a local probe of the ion on the B site and its TM neighbors or a more extended probe, 50% of the Fe(CN)$_6$ entities were replaced by the Cr(CN)$_6$ ones in NiFe. This compound is called NiCr$_{0.50}$Fe$_{0.50}$ in the following and its X-ray diffraction pattern, FC-ZFC magnetization curves and magnetic field dependence of the magnetization at 4 K are shown in S6–S8. The XMCD signals of NiCr$_{0.50}$Fe$_{0.50}$ were compared to

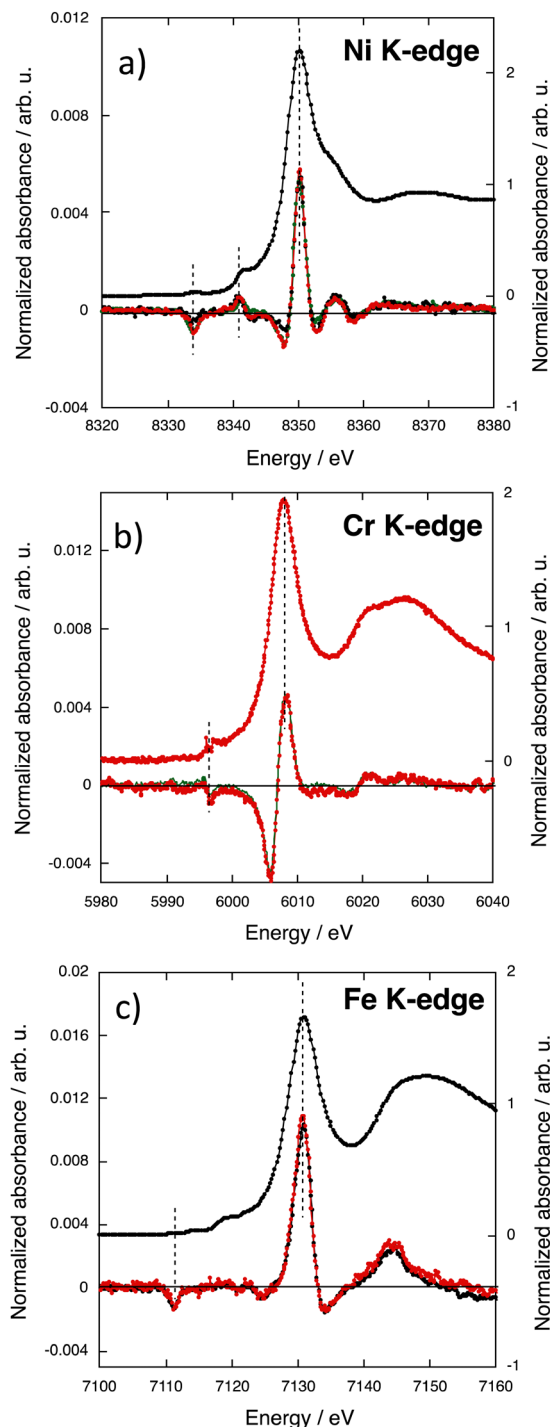**Fig. 7** (a) XMCD signals at the Ni-K edge of NiFe (black), NiCr$_{0.50}$Fe$_{0.50}$ (red) and NiCr (green) and XANES at the Ni K-edge of NiFe (black); (b) XMCD signals at the Cr K-edge of NiCr$_{0.50}$Fe$_{0.50}$ (red) and NiCr (green) and XANES at the Cr K-edge of NiCr$_{0.50}$Fe$_{0.50}$ (red); (c) XMCD signals at the Fe K-edge of NiCr$_{0.50}$Fe$_{0.50}$ (red) and NiFe (black) and XANES at the Fe K-edge of NiFe (black).

those of NiFe and the NiCr PBA (called NiCr) of chemical formula Ni$_4$[Cr(CN)$_6$]$_{8/3}$·17H$_2$O, the synthesis and characterization of which are both presented in ref. 36. Fig. 7a shows the XMCD signals at the Ni K-edge of NiFe, NiCr$_{0.50}$Fe$_{0.50}$ and NiCr.

As expected, the signals are the same. XMCD at the TM ion on the A site of PBAs is a local probe of the ion, which is in a very close environment in the three PBAs, with definitely no influence from the TM ions in the B sites. Fig. 7b and c show the XMCD signals of NiCr$_{0.50}$Fe$_{0.50}$ compared to those of NiCr at the Cr K-edge and of NiFe at the Fe K-edge, respectively. The XMCD signal of NiCr$_{0.50}$Fe$_{0.50}$ is the same as that of NiCr at the Cr K-edge and the same as that of NiFe at the Fe K-edge. This result shows that, as at the K-edge of the TM ions on the A site, XMCD at the K-edge of the TM ions on the B site is not sensitive to the replacement of part of them and is therefore a local probe of the ion at the B site and its first metallic neighbors.

2. **XMCD at the TM K-edge, a probe extremely sensitive to very slight structural distortions.** Variable pressure XMCD measurements at the Ni and Fe K-edges of NiFe at 4 K already showed that XMCD at the TM K-edge is very sensitive to slight structural distortions.[18] This high sensitivity arises from the symmetry dependent mixing of the 3d and 4p orbitals. As discussed above, the higher intensity of the 1s → 4p XMCD signal at the Co and Ni K-edges of Co$_{0.35}$Ni$_{0.65}$Fe is most likely caused by a slight distortion of the Co and the Ni sites due to network strains arising from the accommodation of ions of different sizes in the same sublattice of the PBA. No such effect is observed at the Fe K-edge of this compound. This is expected as the Fe(CN)$_6$ entity, in which the Fe^{3+} ion is low spin, is made of stronger and more covalent bonds than the Co^{2+} and Ni^{2+} high spin-to-ligand bonds. X-ray absorption near edge spectra (XANES) is a probe of the local structure around the absorbing atom. The XANES spectra of Co$_{0.35}$Ni$_{0.65}$Fe were recorded at the Co, Ni and Fe K-edges and compared to those of CoFe and NiFe; they are shown in Fig. 8. Fig. 8 shows that, whatever the K-edge, the XANES spectra of Co$_{0.35}$Ni$_{0.65}$Fe are very close to those of CoFe and of NiFe. The distortion of the Co^{2+} and Ni^{2+} sites is probably too small to be detectable on the XANES spectra at the TM K-edge. This therefore shows that XMCD at the TM K-edge could turn out to be an unprecedented tool to detect and analyze very slight distortions affecting magnetic sites.
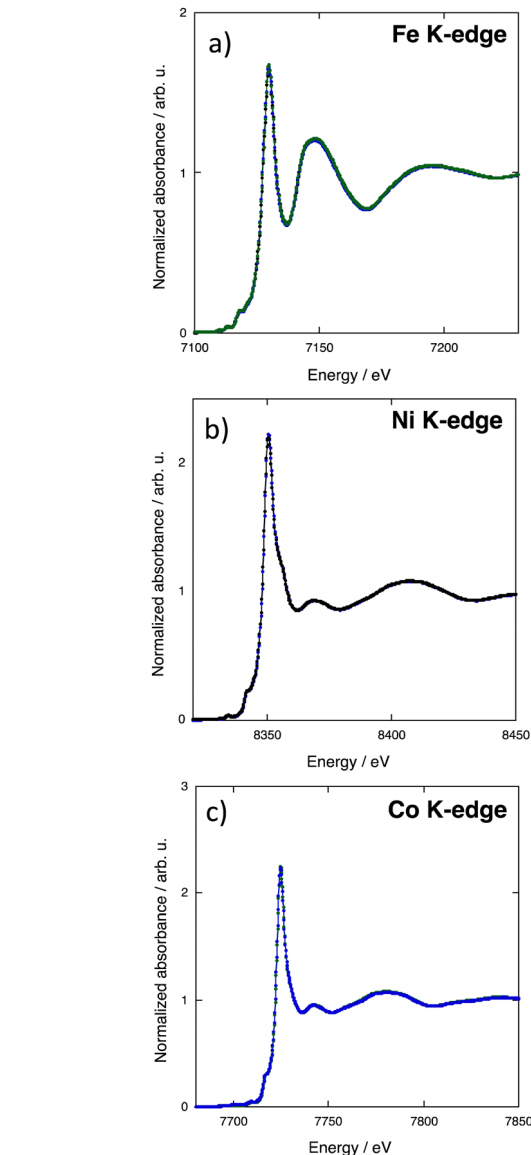

Fig. 8 (a) XANES spectra at the Fe K-edge of Co$_{0.35}$Ni$_{0.65}$Fe (blue), CoFe (green) and NiFe (black); (b) XANES spectra at the Ni K-edge of Co$_{0.35}$Ni$_{0.65}$Fe (blue) and NiFe (black) (c) XANES spectra at the Co K-edge of Co$_{0.35}$Ni$_{0.65}$Fe (blue) and CoFe (green).

Experimental

A series of five (Co$_x$Ni$_{(1-x)}$)$_4$[Fe(CN)$_6$]$_{8/3}$·nH$_2$O PBAs (called Co$_x$Ni$_{(1-x)}$Fe) were synthesized. EDS analysis, powder X-ray diffraction and magnetic measurements were performed using the devices of the ICMMO instrumentation platform. The syntheses and characterizations of the two extreme compounds CoFe and NiFe were presented in ref. 36.

Sample preparation

The three PBAs were synthesized by drop-by-drop addition of two precursors in aqueous solutions: a 400 mL aqueous solution of potassium hexacyanoferrate(III) K$_3$[Fe(CN)$_6$] (c = 2.5 × 10^{-3} mol L^{-1}) was added to a 100 mL aqueous solution of a mixture of Co(NO$_3$)$_2$ and Ni(NO$_3$)$_2$ salts (c_{tot} = 50 × 10^{-3} mol L^{-1}). The precipitates were washed with distilled water and centrifuged three times at 8000 rpm and finally allowed to dry in air at room temperature.

Energy dispersive spectroscopy (EDS) analysis

The chemical formulas of the three trimetallic PBAs were determined by EDS analysis, using an EDS spectrometer installed on a ZEISS Sigma HD microscope. Data processing was done using the IDFix EDS analysis software. The results are given in S1 (ESI†) for the Co$_x$Ni$_{(1-x)}$Fe series.

Powder X-ray diffraction (XRD)

Powder XRD data were collected with a Philips X'Pert diffractometer (Cu Kα$_1$ radiation) at room temperature. All diagrams were recorded over the 10–70° 2θ angle range with steps of 0.01°.

This journal is © the Owner Societies 2024

Phys. Chem. Chem. Phys., 2024, 26, 15576–15586 | 15583

An aluminum sample holder was used for all measurements. The cell parameters were extracted by a Le Bail refinement procedure (using the Fullprof software), considering an $Fm3m$ space group. The XRD patterns and corresponding cell parameters of the $Co_xNi_{(1-x)}Fe$ series are given in S1 (ESI†).

SQUID magnetometry

Magnetic properties were investigated using a quantum device XL-7 SQUID magnetometer. 5.6 mg of PBA powder was placed in a capsule and 17 mg of eicosane were added to ensure that the particles would not move with the application of the magnetic field. Field cooled-zero field cooled (FC-ZFC) measurements were performed over the 2—100 K temperature range under a 30 Oe magnetic field (S2, ESI†). In order to determine the Weiss temperature (θ), the magnetization was measured as a function of temperature up to 300 K under a 5000 Oe magnetic field; the experimental curves were fitted using a Curie–Weiss law (S3, ESI†). Finally, the magnetic field dependence of magnetization was recorded at 4 K for a magnetic field varying between $-40\,000$ Oe (-4 T) and $40\,000$ Oe (4 T).

Transition metal K-edge XAS

X-ray absorption spectra in the transmission mode were recorded for the $Co_xNi_{(1-x)}Fe$ series at the three K-edges on the SAMBA beamline[56] at SOLEIL (Gif sur Yvette, France). We used a Si(220) monochromator and recorded the spectra in a continuous mode. Measurements were performed at room temperature on pellets. We carefully checked that no radiation damage occurred. Following the measurements, the spectra were energy-calibrated and conventionally normalized using the ATHENA software.[57]

TM K-edge XMCD

Co, Ni and Fe K-edge X-ray absorption near-edge structure (XANES) spectra and XMCD signals were recorded in the transmission mode using the dispersive setup of the ODE beamline[58,59] at SOLEIL synchrotron (Gif sur Yvette, France). Detailed information is given about the measurements and normalization procedure in ref. 35, and so only the main ones are reminded here. The circular polarization rate is the same for all the edges. The Si(311) polychromator was chosen to achieve the highest possible resolution in the white line region of the spectra. Then, it is critical (i) to be well below the Curie temperature of the eight investigated PBAs, and (ii) to avoid any artifact in the intensity related to a change in the temperature, we carefully performed the measurements at 4 K. The largest external magnetic field (1.3 T) that can be reached when the cryostat was used was applied alternatively parallel and anti-parallel to the direction of the photon beam. The samples were placed in a diamond anvil cell (DAC) and, to minimize the absorption of the beam while retaining a brilliant enough flux to be able to perform the measurements, the diamonds of the DAC were replaced by Plexiglas strips. No radiation damage occurred thanks to attenuators of appropriate thickness. A metallic foil was recorded at both edges for energy calibration.

We normalized the XANES spectra and XMCD signals using the procedure described in ref. 35.

Conclusions

The study of the trimetallic $Co_xNi_{(1-x)}Fe$ PBA series by TM K-edge XMCD at the Co, Ni and Fe K-edges and SQUID magnetometry shows that their magnetic structures can be explained by exchange interactions of the same sign as seen in the corresponding binary PBAs and spin frustration is not expected to occur.

Local structural distortions are likely to occur at certain compositions that cannot be detected by XAS but can be detected by XMCD, indicating that K-edge XMCD could be an extremely sensitive probe of slight structural distortions.

The use of the trimetallic $Co_xNi_{(1-x)}Fe$ PBA series as a tool to better understand the TM K-edge XMCD in PBAs shows that K-edge XMCD is a local atomic probe of the TM atoms probed in this PBA series, despite the spatially extended character of the probed 4p orbitals. At the A site, TM K-edge XMCD is an atomic probe of only the probed element. At the B site, due to the deviation from centro-symmetry of the A site and the associated 3d–4p mixing,[38] XMCD at the TM K-edge is a local probe of the probed element but also of its first magnetic neighbors.

The Prussian blue analogues have been chosen as model compounds to better understand TM K-edge XMCD, because some electronic and structural parameters can be selectively varied and were successfully related to XMCD features. The next step will be to extend the interpretation of the TM K-edge XMCD signals of PBAs to (i) other molecular magnetic materials and (ii) materials whose electronic structures are well-described in terms of molecular orbitals. Another step will be to get direct experimental evidence of our hypothesis on the relative orientation of the magnetic moments and crystallographic axes (ref. 36 and 38 and this work). Resonant X-ray scattering using circularly polarized X-rays or neutron diffraction could be performed to get such evidence.

Author contributions

The authors are sad to specify that their colleague, co-author and friend, François Baudelet, passed away on January 28th, 2022. He carried out the experiments during two synchrotron beamtimes for the results presented here and was deeply involved in the interpretation of the data. The manuscript was written through the contribution of all other authors, who have given approval to the final version of the manuscript.

Conflicts of interest

There are no conflicts to declare.

15584 | *Phys. Chem. Chem. Phys.*, 2024, **26**, 15576–15586

This journal is © the Owner Societies 2024

Acknowledgements

Notes and references

1 B. T. Thole, P. Carra, F. Sette and G. van der Laan, *Phys. Rev. Lett.*, 1992, **68**, 1943.

2 P. Carra, B. T. Thole, M. Altarelli and X. Wang, *Phys. Rev. Lett.*, 1993, **70**, 694.

3 C. T. Chen, Y. U. Idzerda, H.-J. Lin, N. V. Smith, G. Meigs, E. Chaban, G. H. Ho, E. Pellegrin and F. Sette, *Phys. Rev. Lett.*, 1995, **75**, 152.

4 R. Moroni, C. Cartier dit Moulin, G. Champion, M.-A. Arrio, P. Sainctavit, M. Verdaguer and D. Gatteschi, *Phys. Rev. B: Condens. Matter Mater. Phys.*, 2003, **68**, 064407.

5 A. Rogalev and F. Wilhelm, *Phys. Metals Metallography*, 2015, **116**, 1285.

6 J. I. Igarashi and K. Hirai, *Phys. Rev. B: Condens. Matter Mater. Phys.*, 1996, **53**, 6442.

7 N. Bouldi, N. J. Vollmers, C. G. Delpy-Laplanche, Y. Joly, A. Juhin, P. Sainctavit, C. Brouder, M. Calandra, L. Paulatto, F. Mauri and U. Gerstmann, *Phys. Rev. B*, 2017, **96**, 085123.

8 H. Ebert, *Solid State Commun.*, 1996, **100**, 677.

9 S. Stähler, G. Schütz and H. Ebert, *Phys. Rev. B*, 1993, **47**, 818.

10 H. J. Gotsis and P. A. Strange, *J. Phys.: Condens. Matter*, 1994, **6**, 1409.

11 G. Y. Guo, *J. Phys.: Condens. Matter*, 1996, **8**, L747.

12 C. Brouder and M. Hikam, *Phys. Rev. B: Condens. Matter Mater. Phys.*, 1991, **43**, 3809.

13 C. Brouder, M. Alouani and K. H. Bennemann, *Phys. Rev. B: Condens. Matter Mater. Phys.*, 1996, **54**, 7334.

14 C. R. Natoli, M. Benfatto and S. Doniach, *Phys. Rev. A: At., Mol., Opt. Phys.*, 1986, **34**, 4682.

15 Y. Joly, O. Bunau, J. E. Lorenzo, R. M. Galéra, S. Grenier and B. Thompson, *J. Phys.: Conf. Ser.*, 2009, **190**, 012007.

16 R. Torchio, O. Mathon and S. Pascarelli, *Coord. Chem. Rev.*, 2014, **277–278**, 80.

17 F. Baudelet, S. Pascarelli, O. Mathon, J.-P. Itié, A. Polian, M. d'Astuto and J.-C. Chervin, *J. Phys.: Condens. Matter*, 2005, **17**, S957.

18 J.-D. Cafun, J. Lejeune, J.-P. Itié, F. Baudelet and A. Bleuzen, *J. Phys. Chem. C*, 2013, **117**, 19645.

19 N. Ishimatsu, T. Shichijo, Y. Matsushima, H. Maruyama, Y. Matsuura, T. Tsumuraya, T. Shishidou, T. Oguchi, N. Kawamura, M. Mizumaki, T. Matsuoka and K. Takemura, *Phys. Rev. B: Condens. Matter Mater. Phys.*, 2012, **86**, 104430.

20 R. Torchio, Y. O. Kvashnin, S. Pascarelli, O. Mathon, C. Marini, L. Genovese, P. Bruno, G. Garbarino,

A. Dewaele, F. Occelli and P. Loubeyre, *Phys. Rev. Lett.*, 2011, **107**, 237202.

21 R. Torchio, A. Monza, F. Baudelet, S. Pascarelli, O. Mathon, E. Pugh, D. Antonangeli and J.-P. Itié, *Phys. Rev. B: Condens. Matter Mater. Phys.*, 2011, **84**, 060403(R).

22 G. Schütz, W. Wagner, W. Wilhelm, P. Kienle, R. Zeller, R. Frahm and G. Materlik, *Phys. Rev. Lett.*, 1987, **58**, 737.

23 J. P. Rueff, R. M. Galéra, C. Giorgetti, E. Dartyge, C. Brouder and M. Alouani, *Phys. Rev. B: Condens. Matter Mater. Phys.*, 1998, **58**, 12271.

24 J. Herrero-Albillos, F. Bartolomé, L. M. Garcia, P. Cerbuna, F. Casanova, A. Labarta and X. Batlle, *Phys. Rev. B: Condens. Matter Mater. Phys.*, 2007, **75**, 187402.

25 M. A. Laguna-Marco, C. Piquer and J. Chaboy, *Phys. Rev. B: Condens. Matter Mater. Phys.*, 2009, **80**, 144419.

26 V. Gadet, T. Mallah, I. Castro, M. Verdaguer and P. Veillet, *J. Am. Chem. Soc.*, 1992, **114**, 9213.

27 T. Mallah, S. Thiébaut, M. Verdaguer and P. Veillet, *Science*, 1993, **262**, 1554.

28 S. Ferlay, T. Mallah, R. Ouahès, P. Veillet and M. Verdaguer, *Nature*, 1995, **378**, 701.

29 T. Mallah, S. Ferlay, C. Auberger, C. Hélary, F. L'Hermite, R. Ouahès, J. Vaissermann, M. Verdaguer and P. Veillet, *Mol. Cryst. Liq. Cryst.*, 1995, **273**, 141.

30 M. Verdaguer, T. Mallah, C. Hélary, F. L'Hermite, P. Sainctavit, M.-A. Arrio, D. Babel, F. Baudelet, E. Dartyge and A. Fontaine, *Phys. B*, 1995, **208–209**, 765.

31 E. Dujardin, S. Ferlay, X. Phan, C. Desplanches, C. Cartier dit Moulin, P. Sainctavit, F. Baudelet, E. Dartyge, P. Veillet and M. Verdaguer, *J. Am. Chem. Soc.*, 1998, **120**, 11347.

32 J. M. Herrera, A. Bachschmidt, F. Villain, A. Bleuzen, V. Marvaud, W. Wernsdorfer and M. Verdaguer, *Phil. Trans. R. Soc. A*, 2008, **366**, 127.

33 G. Champion, V. Escax, C. Cartier dit Moulin, A. Bleuzen, F. Villain, F. Baudelet, E. Dartyge and M. Verdaguer, *J. Am. Chem. Soc.*, 2001, **123**, 12544.

34 A. Bordage, L. Nataf, F. Baudelet and A. Bleuzen, *J. Phys.: Conf. Ser.*, 2016, **712**, 012109.

35 A. N'Diaye, A. Bordage, L. Nataf, F. Baudelet, T. Moreno and A. Bleuzen, *J. Synchrotron Rad.*, 2021, **28**, 1127.

36 A. N'Diaye, A. Bordage, L. Nataf, F. Baudelet, E. Rivière and A. Bleuzen, *Inorg. Chem.*, 2022, **61**, 6326.

37 A. Bordage, A. N'Diaye and A. Bleuzen, *C. R. Chimie*, 2022, **25**, 281.

38 A. N'Diaye, A. Bordage, L. Nataf, F. Baudelet, E. Rivière and A. Bleuzen, *ACS Omega*, 2022, 7, 36366.

39 S.-I. Ohkoshi, T. Iyoda, A. Fujishima and K. Hashimoto, *Phys. Rev. B: Condens. Matter Mater. Phys.*, 1997, **56**, 11642.

40 S.-I. Ohkoshi, O. Sato, T. Iyoda, A. Fujishima and K. Hashimoto, *Inorg. Chem.*, 1997, **36**, 268.

41 S.-I. Ohkoshi, S. Yorozu, O. Sato, T. Iyoda, A. Fujishima and K. Hashimoto, *Appl. Phys. Lett.*, 1997, **70**, 1040.

42 S.-I. Ohkoshi, O. Sato, A. Fujishima and K. Hashimoto, *J. Am. Chem. Soc.*, 1998, **120**, 5349.

This journal is © the Owner Societies 2024

Phys. Chem. Chem. Phys., 2024, **26**, 15576–15586 | **15585**

43 S.-I. Ohkoshi and K. Hashimoto, *Phys. Rev. B: Condens. Matter Mater. Phys.*, 1999, **60**, 12820.

44 S.-I. Ohkoshi and K. Hashimoto, *J. Am. Chem. Soc.*, 1999, **121**, 10591.

45 A. Widmann, H. Kahlert, I. Petrovic-Prelevic, H. Wulff, J. V. Yakhmi, N. Bagkar and F. Scholz, *Inorg. Chem.*, 2002, **41**, 5706.

46 A. Kumar and S. M. Yusuf, *Phys. B*, 2005, **362**, 278.

47 L. Egan, K. Kamenev, D. Papanikolaou, Y. Takabayashi and S. Margadonna, *J. Am. Chem. Soc.*, 2006, **128**, 6034.

48 D. M. Pajerowski, J. E. Gardner, D. R. Talham and M. W. Meisel, *J. Am. Chem. Soc.*, 2009, **131**, 12927.

49 D. M. Pajerowski, T. Yamamoto and Y. Einaga, *Inorg. Chem.*, 2012, **51**, 3648.

50 F. J. Luque, I. A. Kowalik, J. P. Prieto-Ruiz, M. A. Nino, H. Prima-Garcia, F. M. Romero, D. Arvanitis, E. Coronado, R. Miranda and J. J. de Miguel, *J. Mater. Chem. C*, 2018, **6**, 8171.

51 S. F. Jafri, M.-A. Arrio, A. Bordage, R. Moulin, A. Juhin, C. Cartier dit Moulin, E. Otero, P. Ohresser, A. Bleuzen and P. Sainctavit, *J. Inorg. Chem.*, 2018, **57**, 7610.

52 M. Atanasov, P. Comba, C. A. Daul and A. Hauser, *J. Phys. Chem. A*, 2007, **111**, 9145.

53 J. S. Smart, *Effective Field Theory of Magnetism*, W. B. Saunders Company, Philadelphia and London, 1966.

54 J. E. Greedan, *J. Mater. Chem.*, 2001, **11**, 37.

55 A. Kumar, S. M. Yusuf, L. Keller and J. V. Yakhmi, *Phys. Rev. Lett.*, 2008, **101**, 207206.

56 V. Briois, E. Fonda, S. Belin, L. Barthe, C. La Fontaine, F. Langlois, M. Ribens and F. Villain, *UVX 2010 EDP Sci.*, 2011, 41.

57 B. Ravel and M. Newville, *J. Synchrotron Rad.*, 2005, **12**, 537.

58 F. Baudelet, Q. Kong, L. Nataf, J.-D. Cafun, A. Congedutti, A. Monza, S. Chagnot and J.-P. Itié, *High Press. Res.*, 2011, **31**, 136.

59 F. Baudelet, L. Nataf and R. Torchio, *High Press. Res.*, 2016, **36**, 429.

15586 | *Phys. Chem. Chem. Phys.*, 2024, **26**, 15576–15586

This journal is © the Owner Societies 2024